Characterization of Microscale Material Behavior with MEMS Resonators

C. White, R. Xu, X. Sun, and K. Komvopoulos
Department of Mechanical Engineering, University of California, Berkeley, CA 94720

ABSTRACT

For reliable MEMS device fabrication and operation, there is a continued demand for precise characterization of materials at the micron scale. This paper presents a novel material characterization device for fatigue lifetime testing. The fatigue specimen is subjected to multi-axial loading, which is typical of most MEMS devices. In order to generate a sufficiently large stress, the fatigue devices were tested in resonance to produce a maximum von Mises equivalent stress as high as 1 GPa, which is in the fracture strength range reported for polysilicon. A further increase of the stress in the beam specimens was obtained by introducing a notch with a focused ion beam. The notch resulted into a stress concentration factor of about 3.8, thereby producing maximum von Mises equivalent stress in the range of 1–4 GPa. This study provides insight into multi-axial fatigue testing under typical MEMS conditions and additional information about micron-scale polysilicon mechanical behavior, which is the current basic building material for MEMS devices.

Keywords: fatigue, microscale material characterization, resonator, polysilicon, microelectromechanical systems (MEMS).

1 INTRODUCTION

Progress in microelectromechanical systems (MEMS) has led to the use of miniaturized devices in various civil and military applications. However, several obstacles must be overcome before micromachine technology could benefit society. MEMS reliability is of particular importance, specifically basic understanding of material behavior at the microscale. Accelerated life testing, estimation of damage during operation, and microscale material behavior are essential to the design of inertial systems, deformable surfaces for vehicle control, multi-arrays capable of sensing deformation in highly-stressed components, microsensors for harsh environments, and high-resolution microdisplays. To increase the reliability and longevity of such microdevices, it is necessary to accurately determine the material response under both static and dynamic loading conditions. Since the strength of brittle materials is scale-dependent (due to the lower probability of flaws and higher-quality surfaces), defect-free microstructures may exhibit higher fatigue resistance. However, in view of their small dimensions, these devices often fail abruptly because fatigue life is determined by crack initiation, which is microstructure sensitive.

Information about microscale fatigue is rather limited, probably due to the lack of appropriate instrumentation and specimens to simulate loading conditions encountered in microdevices. Therefore, a significant scatter in the fatigue strength of thin polycrystalline silicon (polysilicon) elements is not uncommon. Experiments have been performed using a number of different techniques including strain-controlled tensile tests with polysilicon specimens [1], fracture tests with silicon microcantilever beams [2,3], electrostatic actuation and capacitive sensing of motion to study the fatigue behavior of notched cantilever-type polysilicon specimens excited in resonance and correlated the fatigue life to the stress amplitude at the notch root [4], pre-cracked single-crystal silicon cantilevers tested at resonance by observing the change of the resonance frequency with time [5]. High-cycle fatigue testing of single-crystal silicon films performed in atmospheres containing water vapor showed premature failure at cyclic stress about one-half of the single-crystal fracture strength [6].

Despite valuable insight into microscale mechanical properties of polysilicon obtained in previous studies, the simple devices used in most experiments did not simulate fatigue under the multiaxial loading conditions such as those encountered in MEMS. Micromachine devices are subjected to billions of mixed-loading cycles. The microdevice used in this work has a unique multiaxial loading state induced during cycling. Furthermore, the use of probe tips or load cells to apply a force on microfabricated test specimens introduces significant errors in force measurements because it is difficult to accurately determine the microscopic displacement of a macroscopic device. Therefore, on-chip actuation of the microscopic test specimen using electrostatic actuation was employed in this work because it provides greater load control compared to macroscopic methods. The main objective of this work was to examine the evolution of fatigue damage in polysilicon MEMS resonators due to multi-axial loading. To achieve this goal, a fatigue microdevice was designed and fabricated using surface micromachining to replicate real world loading conditions. The design and resonance characteristics of the multi-axial fatigue microdevice are outlined in this paper with emphasis on the dynamic performance of the device. Preliminary stress-life fatigue results are also discussed for devices tested in ambient and vacuum conditions.

2 MULTI-AXIAL FATIGUE DEVICES

2.1 Design and Fabrication

Multi-axial fatigue devices were fabricated using surface micromachining techniques in the multi-user MEMS processes (MUMPs) of the JDS Uniphase MEMS business unit (Cronos). A ground plane layer and structural layer of polysilicon, and two sacrificial layers were used to build the devices. Backend processing released the fatigue structures, removing the $Si0_2$ sacrificial layer and ensuring free movement of the structures while keeping the integrity of the polysilicon structures. The chips were dried using critical point drying (maximum pressure of 1250 psi and maximum temperature of 40 °C), in order to minimize the likelihood of stiction-induced failure.

Figure 1 shows a scanning electron microscopy (SEM) micrograph of a multi-axial fatigue device. In this device, on-chip actuation is provided by comb drives, which generate the necessary electrostatic force to rotate the structure. The comb drives are arranged along radial "spokes" extending from a suspended ring that is held in place by thin beams attached to the ring on one end and anchored to the substrate at the other end. These polysilicon cantilever beams are the fatigue test specimens. Applying a potential difference between the suspended and stationary comb teeth actuates the comb drives, rotating the suspended structure. Five electrical lines were integrated into the design, where one line supplies a DC voltage to the specimen, the hub, and the middle comb fingers. The six comb drives were split into two groups, one for driving and one for sensing, requiring a total of five electrical connections. In addition, for each set, each side of the comb drive was wired so that two signals (out of phase by 180°) could be applied for both driving and sensing. Each side of the comb drive is therefore able to alternate pulling the device, reducing the applied voltage for actuation and also ensuring that the beam remains centered in resonance.

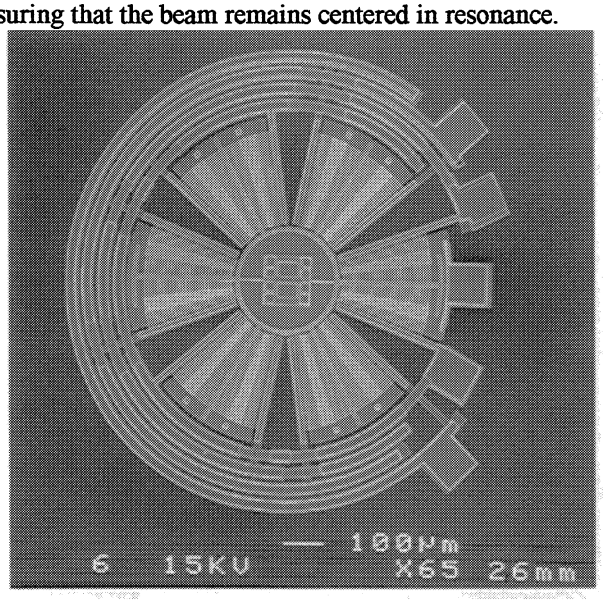

Figure 1: SEM micrograph of multi-axial fatigue device.

Ten different specimen geometries were fabricated to achieve different stress amplitudes and ensure stability while resonating. Two- and three-beam suspended structures were designed with beam lengths ranging from 30 to 80 µm. A list of the tested fatigue devices is given in Table 1.

2.2 Stress Analysis

The schematic at the top of Fig. 2 shows the rotation of the test specimen along the path of the outer ring structure. In this rotation, the beam is subjected to axial extension, shear force, and bending, resulting in a multiaxial state of stress. Contours of the equivalent von Mises stress, calculated using the finite element method, are shown in the lower portion of Fig. 2. Such stress calculations were made and compared for static and dynamic loading. Since variations were not significant, static conditions were used to calculate the maximum equivalent stress for given amplitude given the much shorter computation time required.

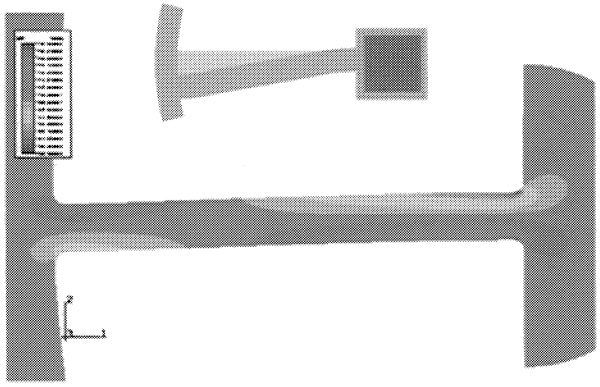

Figure 2: Equivalent von Mises stress contours for 80-µm two-beam fatigue devices.

Table 1: Finite element results of maximum von Mises equivalent stress for each fatigue specimen

	Fatigue specimen dimensions (µm)	Estimated maximum von Mises equivalent stress (GPa)
Two-Beam	30 x 4 x 2	0.65
	40 x 4 x 2	0.72
	50 x 4 x 2	0.73
	60 x 4 x 2	0.68
	70 x 4 x 2	0.60
	80 x 4 x 2	0.51
Three-Beam	50 x 4 x 2	0.97
	60 x 4 x 2	0.91
	70 x 4 x 2	0.80
	80 x 4 x 2	0.68

The maximum von Mises equivalent stress values listed in Table 1 for different beam dimensions were obtained for maximum beam deflection at the end of the suspended

beam equal to 2 μm. This deflection is limited by the design of the comb drive and is achievable in vacuum. Fatigue tests performed in these conditions did not achieve failure (or any noticeable degradation) within 10^{10} cycles (as seen in Fig. 4).

2.3 Notched Specimens

A notch was introduced to the beam specimens by a focused ion beam (FIB) to produce a stress concentration in the devices, which would increase the maximum stress and accelerate fatigue. Figure 3 shows the notch geometry produced near the anchor/beam region by the FIB. It can be seen that the radius of curvature at the notch is much smaller than that obtained by the mask through lithography (seen in the attachment of the beam to the anchor at the top of the micrograph). From finite element analysis, the stress concentration factor obtained for this geometry was found equal to ~3.8. This yielded maximum von Mises equivalent stress values in the range of 1–4 GPa.

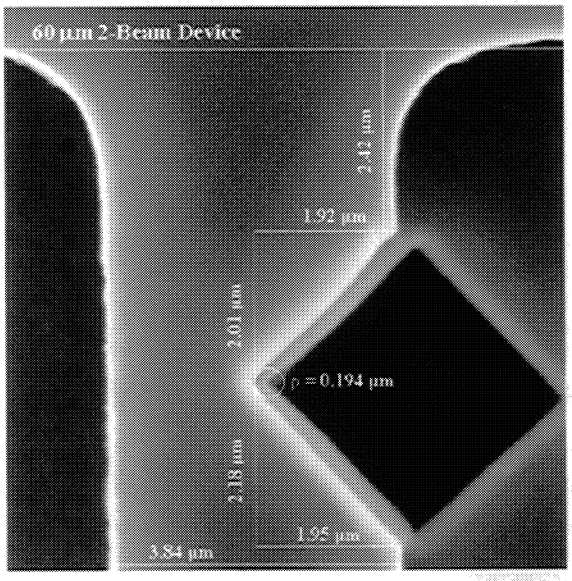

Figure 3: SEM micrograph showing the geometry of a notched fatigue specimen.

3 RESULTS AND DISCUSSION

3.1 Resonance of Fatigue Devices

Devices with different geometries were placed in resonance under ambient conditions and a small decay in resonance frequency was observed. As seen in Fig. 4, over the course of 1 h of testing the resonance frequency decreased from 40 to 90 Hz. The resonance frequencies of the devices ranged from 12 to 35 kHz and comparing this change in resonance frequency to the noise surrounding the system, estimated to be ~4 Hz [7], it can be concluded that the decay cannot be attributed to drift and noise of the system. Hence, while failure was not observed in these test specimens within 10^{10} fatigue cycles, these results illustrate the occurrence of a gradual a fatigue damage process (high-cycle fatigue).

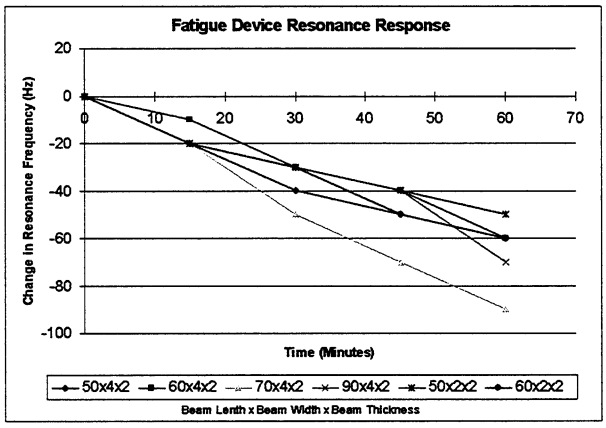

Figure 4: Resonance frequency decay of different fatigue devices tested in ambient air.

3.2 Multi-Axial Fatigue Results

To achieve fatigue failure, the notched specimens were tested in vacuum (10^{-2} Torr), where nonlinear behavior was observed. In this case, the devices were oscillated at a frequency other than their natural resonance frequency. The frequency for testing was set to achieve the desired deflection and therefore stress amplitude. This amplitude was determined by visual inspection and results in a range of stress amplitudes due to the tolerance connected with this method. A direct sensing system is being developed and will be integrated upon completion to obtain more accurate amplitude measurements.

With stress concentration factor values in the range of 3–4, produced as a result of the FIB-fabricated notch, test specimens failed by fatigue. Figures 5 and 6 show the resulting fracture profiles and surfaces of four different test specimens. In these tests, a change in the amplitude for the set frequency was not observed, suggesting that the natural resonance frequency was not affected by fatigue damage. While this behavior is characteristic of brittle fracture, it is possible that a slight change in the resonance frequency occurred that was not possible to detect visually. The brittle fracture is illustrated by the relatively smooth texture of the fracture surfaces shown in Fig. 6.

Figure 7 shows stress amplitude versus fatigue life data for different fatigue devices tested in vacuum (10^{-2} Torr). The data reveal a trend similar to that observed in macroscopic fatigue. An endurance limit appears at a maximum stress of ~1.5 GPa. This might explain why achieving fatigue with unnotched specimens was not possible with a cyclic stress amplitude of ~1.0 GPa.

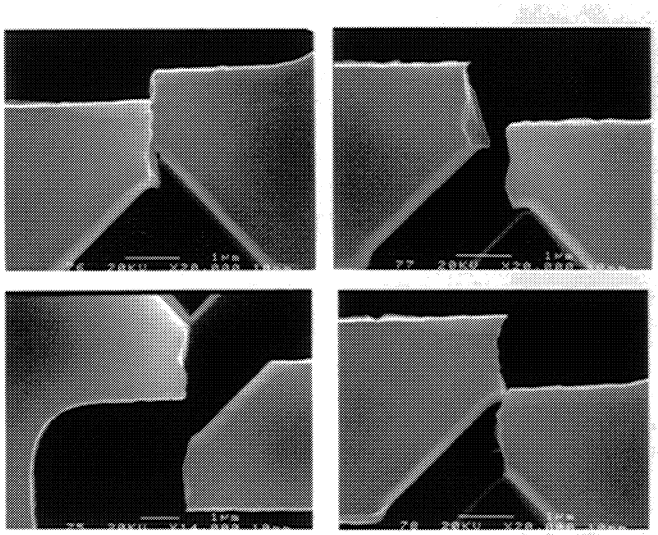

Figure 5: SEM micrographs showing the top view of fractured fatigue beam specimens.

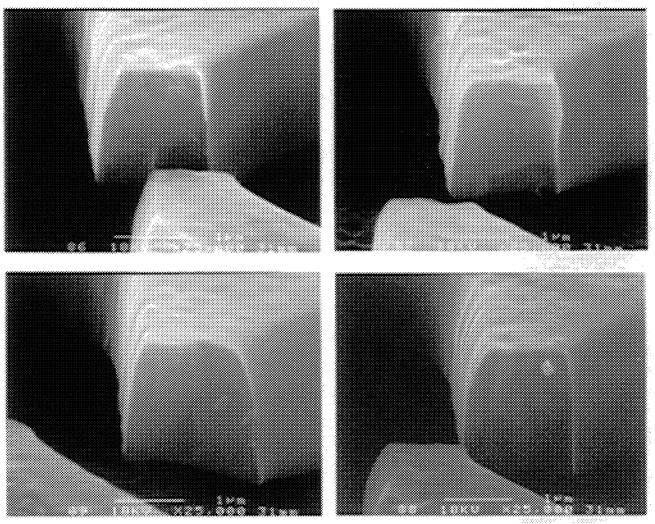

Figure 6: SEM micrographs showing the fracture surfaces of fatigued beam specimens.

When using this curve shown in Fig. 7 a number of different issues must be considered. The stress values are approximate since the amplitude measurements were made visually. In addition, while the notch geometry is fairly consistent, slight variations in notch concentration factors may exist. Since the devices were cycled at very high frequencies, one-second variation may cause the cycles to failure to vary by as much as an order of magnitude. Consequently, the error bars on the data shown in Fig. 7 reflect the uncertainly in the stress calculations. Also shown in Fig. 7 are three data points for unnotched test specimens with beam lengths of 40, 50, and 60 μm (overlapping gray triangles) that did not fail after testing for 10^{10} cycles.

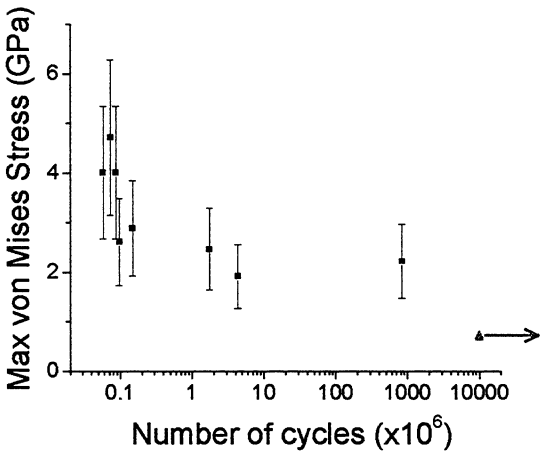

Figure 7: Stress-life curve for two-beam fatigue devices tested in 10^{-2} Torr.

4 CONCLUSIONS

The design and fabrication of a MEMS resonator for performing multi-axial fatigue testing was presented along with preliminary fatigue results. The devices were designed to replicate actual MEMS operating conditions. The necessary stresses for fatigue were achieved by introducing a notch with a focused ion beam that yielded stress concentration factors in the range of 3-4. The obtained stress-life results for polysilicon tested in ambient conditions follow the expected trend, revealing a possible endurance limit for this material close to 1.5 GPa, in agreement with published data. With additional accuracy developed upon the completion of the sensing setup, the present testing scheme and fatigue devices may be used to obtain stress-fatigue life curves for different polysilicon microstructures tested in different environments.

REFERENCES

[1] W. N. Sharpe, B. Yuan, R. Vaidyanathan and B. L., Edwards, Proc. IEEE Micro Electro Mechanical Systems, Nagoya, Japan, Jan. 26-30, 424-429, 1997.

[2] C. J. Wilson, A. Ormeggi and M. Narbutovskih, J. Appl. Phys. 79, 2386-2393, 1996.

[3] C. J. Wilson and P. A. Beck, J. Microelectromechanical Systems 5, 142-150, 1996.

[4] S. B. Brown, W. Van Arsdell and C. L. Muhlstein, Proc. Int. Conf. Solid-State Sensors and Actuators, Transducers '97, Chicago, IL, June 16-19, 591-593, 1997.

[5] J. A. Connally and S. B. Brown, Science 256, 1537-1538, 1992.

[6] C. L. Muhlstein, S. B. Brown and R. O. Ritchie, J. Microelectromechanical Systems 10, pp. 593-600, 2001.

[7] X. Sun, R. Horowitz and K. Komvopoulos, ASME Journal of Dynamic Systems, Measurement, and Control 124, 597-603, 2002.